Hydrothermally synthesised functionalised CuO nanostructures for enhanced thermophysical performance in evacuated tube heat pipes

N. Jayanthi ^{a,b}, M. Venkatesh ^{c*}, R. Suresh Kumar ^d

^a Department of Physics, R.M.K.College of Engineering and Technology, Tiruvallur – 601 206, Tamil Nadu, India

Copper oxide (CuO) nanostructures offer promising potential in solar thermal applications owing to their high thermal conductivity, cost-effectiveness, and structural tunability. In this study, Bare CuO, CuO@EDTA, and CuO@Citrate nanostructures were synthesised via a hydrothermal route and evaluated for their suitability in Evacuated Tube Heat Pipes (ETHPs). Comprehensive characterisation including SEM, XRD, FTIR, and UV-Vis spectroscopy was employed to assess morphology, crystallinity, surface chemistry, and optical absorption behavior. The CuO@EDTA nanostructures exhibited well-aligned anisotropic morphology, highest crystallinity, and a red-shifted absorption edge with a reduced band gap of 4.13 eV. These features translated into improved thermal transport properties. Comparative thermophysical analysis demonstrated that CuO@EDTA nanofluids outperformed Al₂O₃@EDTA and Bare CuO counterparts in terms of thermal conductivity, heat capacity, and flow behavior. The integration of functionalised CuO nanostructures in ETHPs significantly enhanced heat transfer efficiency, suggesting their strong applicability in advanced renewable thermal systems. These findings highlight the role of surface engineering and ligand coordination in optimising nanostructures for nextgeneration energy devices.

(Received July 4, 2025; Accepted October 3, 2025)

Keywords: CuO nanostructures, Hydrothermal synthesis, Nanofluids, Evacuated tube heat pipe, Thermal conductivity, Renewable energy

1. Introduction

The pursuit of efficient thermal management systems has garnered significant attention due to the pressing global demand for sustainable and high-performance energy solutions. Among the diverse range of emerging thermal technologies, Evacuated Tube Heat Pipes (ETHPs) have emerged as a promising avenue for solar thermal applications due to their excellent thermal conductivity, passive operation, and high reliability [1–3]. The integration of nanostructured materials, particularly metal oxide nanoparticles, into these systems has demonstrated potential for enhancing heat transfer efficiency by improving the thermophysical properties of working fluids [4–6].

Copper oxide (CuO) nanoparticles stand out among metal oxides for their superior thermal conductivity, high stability, and ease of synthesis [7–10]. The morphology and surface characteristics of these nanostructures play a pivotal role in determining their effectiveness in heat transfer systems. Hence, controlling the size, shape, and surface functionalization of CuO nanostructures is crucial to optimizing their dispersion stability, thermal conductivity, and compatibility with heat transfer fluids [11–14].

The hydrothermal synthesis method has been widely adopted for producing CuO nanostructures due to its ability to generate highly crystalline, size-controlled, and morphologically

^b Department of Physics, Periyar University, Salem – 636 011, Tamil Nadu, India

^c Department of Physics, K.S. Rangasamy College of Arts and Science (Autonomous), Tiruchengode – 637 215, Tamil Nadu, India

^d Department of Mechanical Engineering, R.M.K. Engineering College, Tiruvallur – 601 206, Tamil Nadu, India

^{*} Corresponding author: venky8086@gmail.com https://doi.org/10.15251/DJNB.2025.204.1177

diverse nanomaterials under relatively mild conditions [15–18]. In recent studies, surface functionalization using organic ligands such as ethylenediaminetetraacetic acid (EDTA) and sodium citrate has demonstrated enhanced stability and performance of CuO nanoparticles in thermal systems [19–21]. These chelating agents not only control particle growth during synthesis but also improve dispersion behavior in aqueous media by modifying surface charges and hydrophilicity [22–25].

Studies have shown that functionalized CuO nanofluids exhibit significant enhancement in thermal conductivity, specific heat capacity, and photothermal conversion efficiency compared to their unmodified counterparts [26–28]. These improvements are attributed to better phonon transport, reduced interfacial resistance, and stable colloidal behavior under dynamic flow conditions, all of which are essential for ETHP applications [29–32].

Furthermore, the optical bandgap of CuO nanostructures can be tuned via surface modification, influencing their light absorption and photothermal response, which is beneficial in solar-assisted heating systems [33–35]. Techniques such as X-ray diffraction (XRD), Fourier-transform infrared spectroscopy (FTIR), and UV–Vis spectroscopy are employed to investigate structural, chemical, and optical characteristics, confirming phase purity, ligand coordination, and bandgap modulation [36–38].

This work aims to synthesise and characterise CuO nanostructures via hydrothermal methods with and without functionalization using EDTA and sodium citrate. We explore their morphology, crystallinity, surface chemistry, optical properties, and thermophysical performance in ETHP systems. The results are expected to contribute toward the development of advanced thermal energy systems, particularly in solar thermal collectors, where nanoparticle-mediated heat transfer enhancement is vital [39–43].

Despite considerable advancements, challenges persist in achieving long-term colloidal stability, minimising viscosity, and maximising energy conversion efficiency of nanofluids in ETHP configurations. Addressing these aspects requires a comprehensive understanding of nanoparticle-ligand interactions, structural tuning, and real-time thermophysical evaluation [44–48].

In this study, we provide a comparative evaluation of Bare CuO, CuO@EDTA, and CuO@Citrate nanostructures, systematically investigating their structural and functional roles in ETHP performance. This multidisciplinary approach bridges nanomaterials science and renewable thermal engineering, aligning with global sustainability goals [49–54].

2. Experimental details

2.1. Materials purchased

All chemicals used in this study were of analytical grade and were used without further purification. Copper(II) sulfate (CuSO₄) and sodium hydroxide (NaOH) were procured from Himedia, while EDTA and sodium citrate (used as a capping agent) were sourced from Merck. Distilled water used throughout the experiments was purchased in 5-litre packs under the brand Fluizds. These materials were obtained from Chemico Glass and Scientific Company, located in Erode. The company is an authorised dealer for leading brands including Merck, Himedia, Sigma-Aldrich, and Isochem.

2.2. Characterization techniques

The synthesised CuO nanostructures were characterised using various analytical techniques to investigate their structure, morphology, and surface functionalities. Phase analysis and crystallite size determination were carried out using a Rigaku SmartLab 9kW XRD, which features a high-flux rotating anode and HyPix-3000 2D semiconductor detector. The θ –2 θ scan mode was employed for powder diffraction studies. Morphological characterisation was performed using a Carl Zeiss Supra 55 VP Field Emission Scanning Electron Microscope (FE-SEM), offering a resolution of 1 nm at 15 kV, equipped with multiple detectors including In-lens and SE2. FTIR was conducted using a JASCO FT/IR6600 (Type A) spectrometer operating over the spectral range of 4000–400 cm⁻¹, with a resolution of 0.4 cm⁻¹, to identify characteristic functional groups

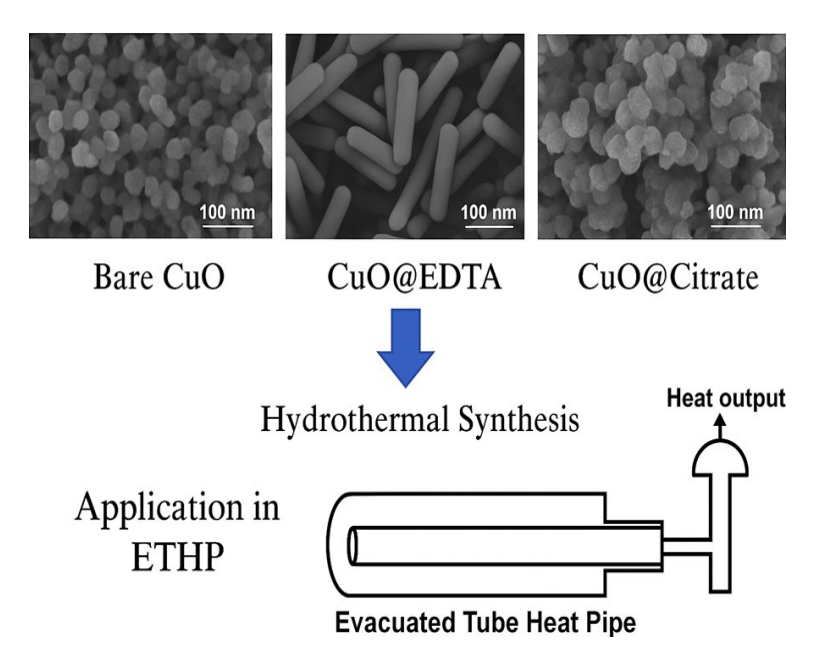
on the nanoparticle surface. Optical absorption and band gap analysis were performed using a Thermo Fisher NanoDrop ND-2000 UV-Vis spectrophotometer, covering a wavelength range of 190-840 nm and requiring a minimum sample volume of $0.5 \,\mu L$.

2.3. Preparation of CuO nanostructures

CuO nanostructures were synthesised via a hydrothermal route. Initially, 1 mmol of CuSO₄ was dissolved in 100 mL of distilled water under continuous stirring. In separate preparations, EDTA and sodium citrate were each dissolved in distilled water and added individually to separate portions of the CuSO₄ solution to act as chelating and capping agents. The solutions were stirred thoroughly to ensure homogeneous mixing. Subsequently, NaOH solution was added dropwise to each mixture to raise the pH to 10, with continuous stirring maintained for 60 minutes at room temperature to facilitate the formation of Cu–ligand complexes. These reaction mixtures were then transferred to Teflon-lined stainless-steel autoclaves and subjected to hydrothermal treatment at 160°C for 4 hours. After cooling to room temperature, the resulting precipitates were collected by centrifugation and washed multiple times with distilled water to remove any residual by-products or unreacted ligands. The cleaned precipitates were dried at 120°C for 3 hours and then calcined at 400°C for 4 hours to improve crystallinity and phase purity. This method yielded Bare CuO, CuO@EDTA, and CuO@Citrate nanostructures, depending on the ligand used during synthesis.

2.4. Sample preparation for ETHPs studies

CuO@EDTA nanopowder, identified as a superior candidate over CuO@Citrate, was selected for nanofluid formulation in ETHP studies. The dried nanostructures were dispersed in distilled water at desired concentrations, and homogeneous suspensions were achieved using ultrasonication with a probe sonicator operating at frequencies between 20 and 40 kHz. This dispersion method avoided the use of surfactants or stabilizing agents, thereby preserving the intrinsic thermophysical properties of the nanofluids. The thermal conductivity, resistivity, volumetric specific heat, and thermal diffusivity of the CuO@EDTA nanofluids were measured using the KD2 PRO Thermal Property Analyzer (Decagon Devices, Inc., USA), a portable, battery-operated device equipped with a stainless-steel needle sensor (60 mm length, 1.27 mm diameter) capable of delivering accurate readings within two minutes across a temperature range of –20°C to 60°C.



Scheme 1. Schematic diagram for the enhanced ETHP efficiency using CuO nanostructures via hydrothermal synthesis.

The prepared nanofluids were subsequently tested in ETHP setups to assess their thermophysical performance under practical thermal operating conditions. As illustrated in Scheme 1, the hydrothermal synthesis of CuO nanostructures followed by functionalisation with EDTA results in enhanced nanoparticle morphology and dispersion stability, which significantly improves heat transfer efficiency when applied in ETHP systems. The schematic visually summarises the synthesis pathway, surface modification, and the resulting application in ETHP configurations, highlighting the role of CuO@EDTA in achieving improved thermal performance for renewable energy technologies.

3. Results and discussion

3.1. Surface morphological evaluation of functionalized CuO nanostructures for ETHP applications

The surface morphology of CuO nanostructures, as revealed by SEM micrographs in Figure 1, highlights the influence of surface functionalization on particle formation and aggregation behavior, which are critical for ETHP applications. The Bare CuO sample exhibits a densely packed, irregular granular morphology composed of aggregated nanocrystallites. These particles lack uniformity and display rough, disordered surfaces, suggesting high surface area but poor dispersion and directional control. Such structural characteristics may hinder efficient thermal transport due to increased interfacial resistance and non-uniform heat distribution.

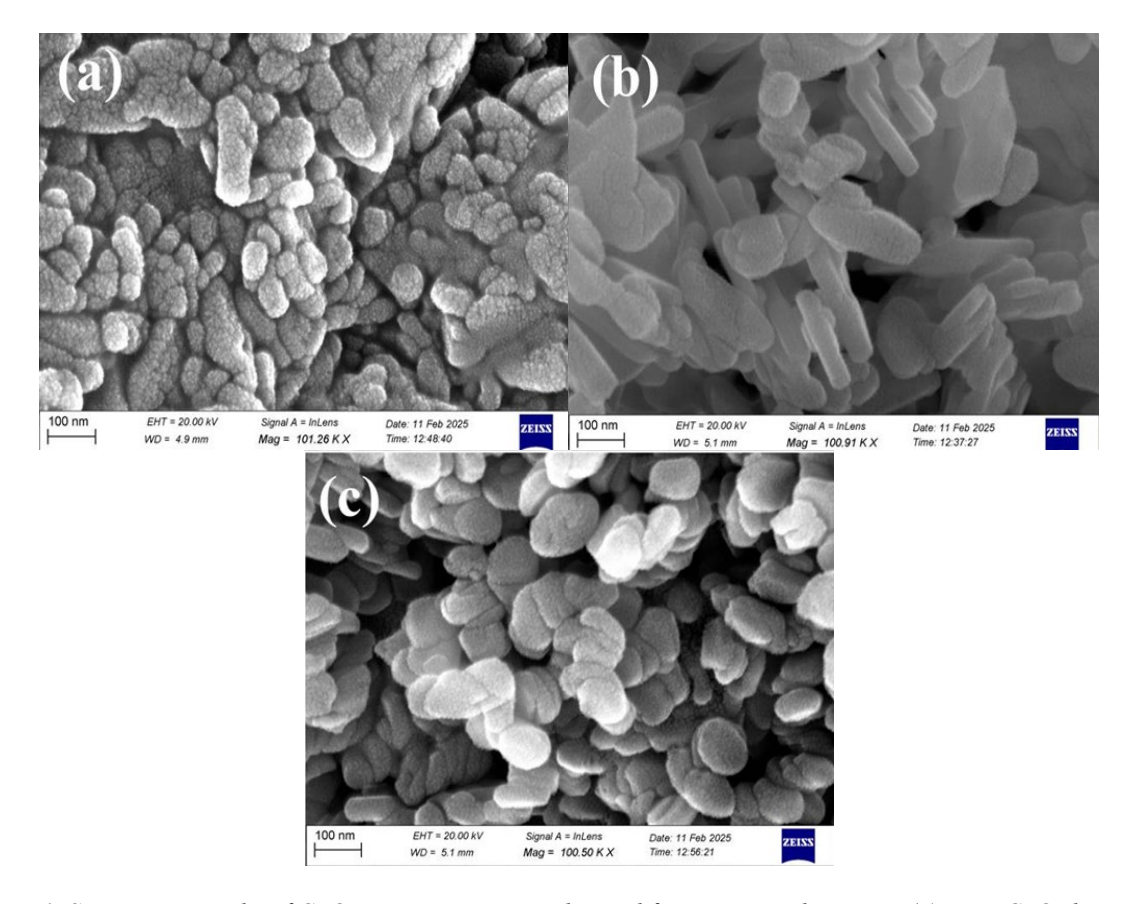


Fig. 1. SEM micrographs of CuO nanostructures synthesised for ETHP applications: (a) Bare CuO showing aggregated and irregular nanocrystallites, (b) CuO@EDTA exhibiting well-aligned rod-like structures with enhanced crystallinity, and (c) CuO@Citrate displaying moderately dispersed, rounded nanostructures.

Scale bar = 100 nm.

In contrast, the CuO@EDTA sample presents a distinct rod-like or plate-like nanostructure with improved alignment and directional growth. The particles appear well-separated and highly anisotropic, reflecting the strong chelating ability of EDTA, which stabilises Cu²⁺ ions during synthesis and promotes controlled nucleation and crystal growth. This organised morphology is expected to enhance phonon transport and fluid–nanoparticle interaction, making it particularly suitable for ETHP systems requiring high thermal conductivity and stable flow dynamics.

The CuO@Citrate sample shows an intermediate morphology, characterised by more uniformly shaped and moderately aggregated nanostructures. The particles are predominantly spherical to oval, with improved surface coverage and partial dispersion. This enhancement in structural organisation is attributed to the moderate chelating nature of citrate, which offers some degree of control over particle formation. While not as structurally refined as CuO@EDTA, the CuO@Citrate nanostructures demonstrate a notable improvement over bare CuO, suggesting a beneficial balance between thermal performance and colloidal stability.

Overall, the morphological evolution from bare CuO to CuO@EDTA reflects the crucial role of surface modifiers in tailoring nanoparticle architecture. Among the three, CuO@EDTA exhibits the most favourable structure for ETHP applications, combining anisotropy, dispersibility, and structural uniformity—all of which are essential for enhancing thermal conductivity and minimising energy losses in advanced heat transfer systems.

3.2. XRD analysis of crystallinity and phase stability in functionalized CuO nanostructures for ETHP applications

The structural characteristics and phase integrity of Bare CuO, CuO@Citrate, and CuO@EDTA nanostructures were rigorously examined using XRD to assess their suitability for ETHP applications. All three samples exhibited distinct diffraction peaks attributable to the monoclinic crystalline structure of CuO, specifically tenorite, which aligns with the JCPDS card No. 45-0937. As illustrated in Figure 2, the primary diffraction peaks occurred at 2θ values of 32.5°, 35.5°, 38.7°, 48.7°, 53.5°, 58.3°, 61.5°, 66.2°, 68.1°, 72.3°, and 75.1°, corresponding respectively to the (110), (-111), (111), (-202), (020), (202), (-113), (311), (220), (311), and (004) crystallographic planes.

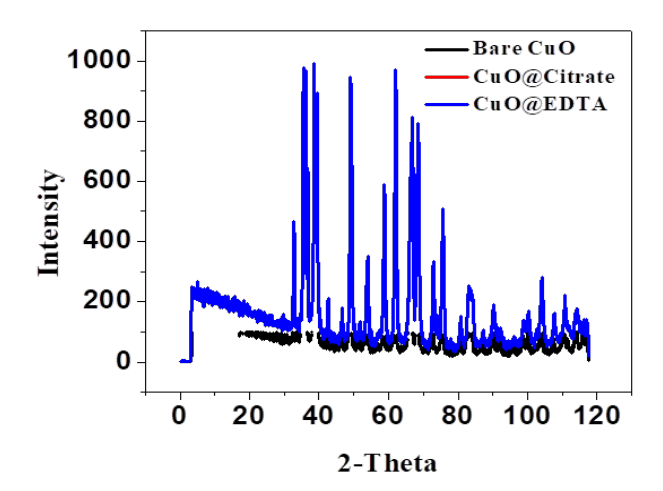


Fig. 2. XRD patterns of Bare CuO, CuO@Citrate, and CuO@EDTA nanostructures for ETHP applications. All samples exhibit characteristic diffraction peaks corresponding to the monoclinic phase of CuO (tenorite), indexed according to JCPDS card No. 45-0937. The prominent reflections are attributed to the (110), (-111), (111), (-202), (020), (202), (-113), (311), (220), (311), and (004) planes. The sharper and more intense peaks observed for CuO@EDTA indicate enhanced crystallinity and increased crystallite size compared to Bare CuO and CuO@Citrate, reflecting improved structural order due to EDTA functionalization.

The XRD profile of Bare CuO displayed moderately broad and less intense peaks, indicative of a smaller crystallite size and moderate crystallinity. Upon surface modification, notable sharpening and intensification of the diffraction peaks were observed—particularly in CuO@EDTA—signifying enhanced crystal growth and improved structural order. The crystallite size was quantitatively estimated using the Debye–Scherrer equation, focusing on the (–111) reflection near $2\theta \approx 35.5^{\circ}$. The progressive decrease in the full width at half maximum (FWHM) from Bare CuO to CuO@EDTA corresponded to an increase in crystallite size, revealing a direct correlation between functionalization and crystal growth.

The calculated crystallite sizes were approximately 10.9 nm for Bare CuO, 14.6 nm for CuO@Citrate, and 29.2 nm for CuO@EDTA. The substantial growth in domain size for CuO@EDTA can be attributed to the strong chelating action of EDTA, which coordinates effectively with Cu²⁺ ions, stabilising the precursor species and facilitating controlled nucleation and crystal development. In comparison, CuO@Citrate exhibited moderate enhancement in both crystallinity and size, consistent with the moderate binding strength of citrate ligands.

Notably, no extraneous peaks corresponding to secondary phases such as Cu_2O or metallic Cu were detected, confirming the high phase purity of the functionalised CuO nanostructures. The preservation of consistent peak positions across all samples underscores that surface functionalisation influenced crystallinity and particle size without disturbing the monoclinic CuO phase structure.

These structural refinements—especially the increase in crystallite size and improved peak resolution—are critically beneficial for ETHP applications. Enhanced crystallinity and larger coherent domains contribute to superior thermal conductivity, mechanical stability, and functional uniformity. Such traits are vital in energy systems, where efficient thermal management and structural integrity of nanomaterials are imperative for long-term performance and reliability.

3.3. Optical absorption and band gap analysis of CuO-based nanostructures for ETHP applications

The optical absorption properties of Bare CuO, CuO@Citrate, and CuO@EDTA nanostructures were thoroughly examined using UV–Visible spectroscopy in the 200–800 nm range to assess their potential for improving solar thermal energy harvesting in ETHP systems. As shown in Figure 3, all samples demonstrated pronounced UV absorption with a prominent peak below 300 nm, corresponding to charge transfer transitions from O²⁻ to Cu²⁺ in the CuO lattice.

The unmodified Bare CuO exhibited an absorption onset at approximately 275 nm, corresponding to a wide optical band gap of 4.51 eV. Citrate modification induced a modest red shift in the absorption edge to ~ 285 nm, reducing the band gap to 4.35 eV. Notably, the CuO@EDTA nanostructure displayed the most significant red shift, with the onset extended to ~ 300 nm and a narrowed band gap of 4.13 eV.

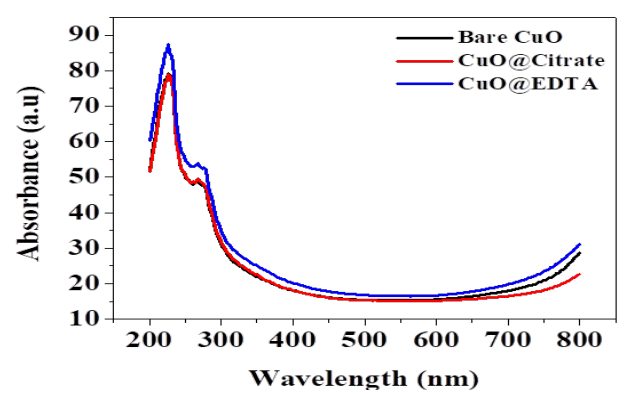


Fig. 3. UV-Visible absorbance spectra of Bare CuO, CuO@Citrate, and CuO@EDTA nanostructures recorded in the wavelength range of 200–800 nm for ETHP applications. The spectra show characteristic UV absorption below 300 nm attributed to $O^{2-} \rightarrow Cu^{2+}$ charge transfer transitions. A progressive red shift in the absorption edge from Bare CuO to CuO@EDTA indicates a reduction in optical band gap due to surface functionalization, with CuO@EDTA exhibiting enhanced absorbance in the visible region.

This progressive shift in optical response and band gap narrowing from Bare CuO to CuO@EDTA underscores the impact of surface functionalization on the electronic properties of CuO nanostructures. EDTA, acting as a potent chelating ligand, likely introduces surface defect states or alters crystallite size, thereby enhancing light absorption in the visible region. Such modifications are highly desirable for ETHP applications, where efficient solar energy capture and photothermal conversion are critical. The improved visible light response of CuO@EDTA suggests its strong potential as an advanced absorber material for next-generation solar thermal systems.

3.4. FTIR spectroscopic analysis of surface functionalization in CuO nanostructures for ETHP applications

FTIR spectroscopy was utilized to evaluate the structural features and surface chemistry of Bare CuO, CuO@Citrate, and CuO@EDTA nanostructures within the 4000–400 cm⁻¹ range, with particular emphasis on their implications for ETHP systems. As shown in Figure 4, all samples exhibit a prominent absorption band between 500–600 cm⁻¹, attributed to Cu–O stretching vibrations, confirming the preservation of the monoclinic CuO phase regardless of surface modification.

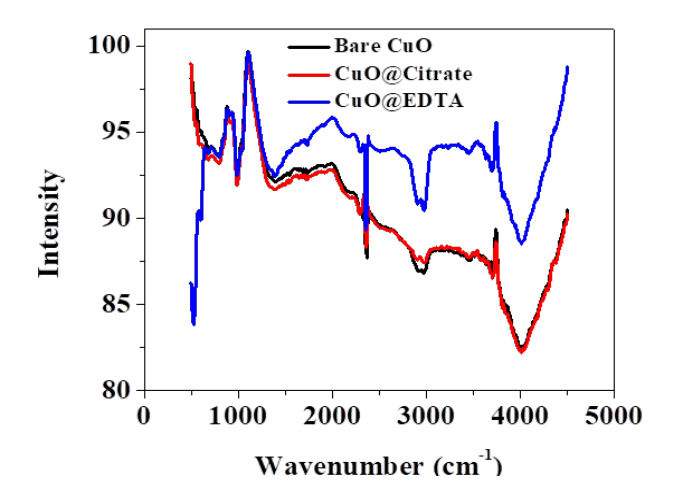


Fig. 4. FTIR spectra of Bare CuO, CuO@Citrate, and CuO@EDTA nanostructures recorded in the range of 4000–400 cm⁻¹ for ETHP applications. The characteristic Cu–O stretching vibrations are evident around 500–600 cm⁻¹ in all samples, confirming the integrity of the CuO lattice. Additional vibrational bands observed in the functionalized samples correspond to carboxylate (-COO⁻), hydroxyl (-OH), and amine (-NH₂) groups, indicating successful surface coordination of citrate and EDTA ligands.

The FTIR spectrum of Bare CuO was relatively featureless beyond the Cu–O region, indicating the absence of surface-bound organic species and confirming the high purity of the unfunctionalized nanostructures. While this purity suggests minimal interference in thermal conduction, the lack of surface groups can result in poor dispersion and sedimentation in heat transfer fluids—an undesirable trait in ETHP systems where stability and uniform thermal transport are critical

Conversely, CuO@Citrate and CuO@EDTA demonstrated significant vibrational bands in the mid-IR region, revealing the successful attachment of organic ligands through surface functionalization. CuO@Citrate showed distinct carboxylate-related bands at ~1570 cm⁻¹ and ~1400 cm⁻¹, attributed to asymmetric and symmetric –COO⁻ stretching vibrations, respectively. These features suggest strong coordination of citrate to the CuO surface, enhancing colloidal stability and compatibility with polar fluids commonly used in ETHP applications. A minor absorption near 2900 cm⁻¹ was observed, corresponding to C–H stretching from alkyl groups in the citrate ligand.

Both functionalized samples exhibited a broad band centered near 3400 cm⁻¹, associated with O-H stretching vibrations due to surface hydroxyl groups or hydrogen-bonded water

molecules. This band was more intense in CuO@EDTA, indicating higher surface hydrophilicity—an advantageous property for enhancing nanoparticle dispersion and thermal conductivity in nanofluids used within ETHPs.

Furthermore, CuO@EDTA displayed additional peaks in the 1000–1700 cm⁻¹ range, including bands ascribed to C–N stretching and N–H bending vibrations, confirming the presence of amine functionalities. These features result from multidentate coordination of EDTA, providing increased surface-active sites and improving nanoparticle stability. Such complexation can facilitate better thermal contact and reduced interfacial resistance in nanofluids, thereby enhancing the efficiency of heat transfer in ETHP operations.

Importantly, the retention of the Cu–O peak position across all samples confirms that surface functionalization does not alter the core crystalline structure of CuO. Instead, it modifies surface chemistry, improving dispersion stability, hydrophilicity, and potential heat exchange performance. These attributes are especially critical in ETHP systems, where consistent and efficient heat transfer relies heavily on the stability and thermophysical behavior of nanofluids under dynamic thermal cycling conditions.

3.5. Comparative analysis of thermophysical properties of CuO@EDTA and Al₂O₃@EDTA nanofluids for ETHP applications

Figure 5 presents a comparative evaluation of the thermophysical properties of Al₂O₃@EDTA and CuO@EDTA nanofluids against their respective counterparts across varying concentrations (3–6%), highlighting their potential for use in ETHP systems such as solar thermal collectors and evacuated tube heat pipes.

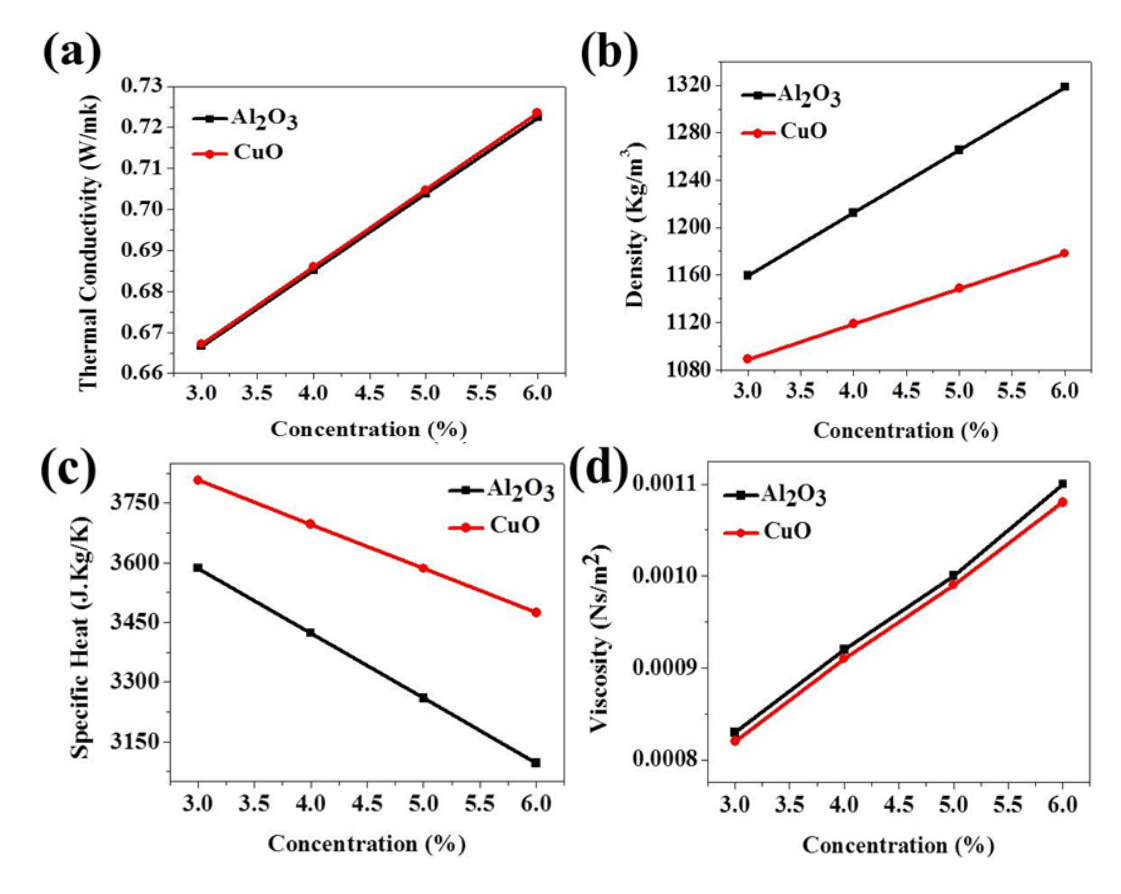


Fig. 5. illustrates the variation of thermophysical properties of Al_2O_3 and CuO nanofluids with increasing nanoparticle concentration (3–6%). Thermal conductivity (a) increases linearly for both fluids, with CuO showing a slight advantage. Density (b) also rises with concentration, with Al_2O_3 nanofluids exhibiting higher values. Specific heat (c) decreases for both nanofluids as concentration increases, but CuO retains comparatively higher values. Viscosity (d) increases steadily, with CuO nanofluids displaying slightly lower viscosity than Al_2O_3 . These trends suggest that CuO nanofluids offer a more favorable combination of thermal and flow properties for advanced heat transfer applications.

Detailed characterisation results for the Al₂O₃ nanostructures are provided in the supplementary information. The findings reveal that both nanofluids exhibit a nearly linear increase in thermal conductivity with increasing nanoparticle concentration. Notably, CuO@EDTA nanofluids consistently display slightly higher thermal conductivity at elevated concentrations, which is primarily attributed to the inherently superior thermal conductivity of CuO and its enhanced dispersibility in the base fluid. These factors collectively facilitate more efficient heat transfer pathways, which are critical for optimal performance in ETHP applications.

In terms of density, both nanofluids show a steady increase as nanoparticle concentration rises. Al_2O_3 nanofluids maintain higher density values across all concentrations, primarily due to the inherently higher density of Al_2O_3 particles and the likelihood of stronger interparticle aggregation. While the increase in density is expected, CuO nanofluids offer a practical advantage with relatively lower density, potentially reducing the pumping power and structural load in thermal systems.

The specific heat capacity of both nanofluids decreases as nanoparticle concentration increases, a well-documented trend arising from the lower specific heat of solid nanostructures compared to that of the base fluid. Despite this general decline, CuO nanofluids consistently retain higher specific heat values than their Al₂O₃ counterparts. This feature is particularly beneficial for applications where thermal energy storage and transient heat buffering are crucial, enabling CuO nanofluids to function not only as efficient heat transfer agents but also as modest thermal reservoirs.

Viscosity increases progressively with nanoparticle loading in both fluid systems, indicating heightened resistance to flow. Notably, CuO nanofluids exhibit slightly lower viscosity than Al₂O₃ nanofluids across all concentrations. This difference, although subtle, can significantly impact the overall energy efficiency of ETHP systems by lowering the pumping power required for circulation and enhancing fluid mobility under operational conditions.

Overall, the comparative trends in thermal conductivity, density, specific heat, and viscosity highlight the superior thermophysical balance offered by CuO nanofluids. While both Al₂O₃ and CuO nanofluids enhance thermal conductivity effectively, CuO formulations deliver an optimised combination of high heat transfer efficiency, moderate density, better heat capacity, and lower viscosity. These properties collectively make CuO nanofluids more attractive candidates for advanced thermal management solutions, especially in systems requiring high thermal responsiveness, low energy consumption, and stable flow behaviour.

4. Conclusion

This study demonstrated the successful synthesis and functionalisation of CuO nanostructures via a hydrothermal method using EDTA and sodium citrate as chelating agents. The resulting nanostructures displayed significant variations in morphology, crystallinity, and optical properties, with CuO@EDTA exhibiting the most favourable characteristics for thermal applications. Detailed structural and spectroscopic analyses confirmed the influence of ligand chemistry on nanoparticle surface features and dispersion behaviour. The thermophysical performance of the synthesised nanofluids, particularly CuO@EDTA, indicated superior thermal conductivity, lower viscosity, and higher specific heat compared to both Bare CuO and Al₂O₃-based counterparts. The improved thermal transport and stability attributes validate the role of surface-engineered CuO nanostructures in enhancing the efficiency of ETHP systems. These findings pave the way for the development of high-performance nanofluids tailored for solar thermal energy harvesting and advanced heat pipe technologies.

References

- [1] Wen D, Ding Y, Int J Heat Mass Transf 49(240-250), 240-250 (2006); https://doi.org/10.1016/j.ijheatmasstransfer.2005.07.009
- [2] Tyagi H, Phelan PE, Prasher R, J Sol Energy Eng 131(041004), 041004 (2009); https://doi.org/10.1115/1.3197562
- [3] Vafai K, Zhu T, Int J Heat Mass Transf 42(2287-2304), 2287-2304 (1999); https://doi.org/10.1016/S0017-9310(98)00017-9
- [4] Eastman JA, Choi SUS, Li S, Yu W, Thompson LJ, Appl Phys Lett 78(718-720), 718-720 (2001); https://doi.org/10.1063/1.1341218
- [5] Chandrasekar M, Suresh S, Int J Heat Mass Transf 54(2559-2570), 2559-2570 (2011).
- [6] Yousefi T, Veysi F, Shojaeizadeh E, Sadaghiani SZ, Int Commun Heat Mass Transf 38(869-874), 869-874 (2011).
- [7] Saidur R, Leong KY, Mohammad HA, Renew Sustain Energy Rev 15(1646-1668), 1646-1668 (2011); https://doi.org/10.1016/j.rser.2010.11.035
- [8] Murshed SMS, Leong KC, Yang C, Appl Therm Eng 29(2109-2125), 2109-2125 (2009); https://doi.org/10.1016/j.applthermaleng.2008.01.005
- [9] Namburu PK, Kulkarni DP, Misra D, Das DK, Exp Therm Fluid Sci 32(397-402), 397-402 (2007); https://doi.org/10.1016/j.expthermflusci.2007.05.001
- [10] Mahian O, Kianifar A, Heris SZ, Wongwises S, Renew Sustain Energy Rev 43(584-598), 584-598 (2015); https://doi.org/10.1016/j.rser.2014.11.020
- [11] Jang SP, Choi SUS, Appl Phys Lett 84(4316-4318), 4316-4318 (2004); https://doi.org/10.1063/1.1756684
- [12] Taylor RA, Otanicar TP, Phelan PE, J Sol Energy Eng 134(021005), 021005 (2012).
- [13] Lee J, Mudawar I, Int J Heat Mass Transf 50(452-463), 452-463 (2007); https://doi.org/10.1016/j.ijheatmasstransfer.2006.08.001
- [14] Xuan Y, Roetzel W, Int J Heat Mass Transf 43(3701-3707), 3701-3707 (2000); https://doi.org/10.1016/S0017-9310(99)00369-5
- [15] Nasrollahzadeh M, Sajadi SM, Khalaj M, J Colloid Interface Sci 508(50-58), 50-58 (2017).
- [16] Liu Y, Yang M, Wei M, Electrochim Acta 178(118-126), 118-126 (2015).
- [17] Yu J, Guo H, Zhang H, Mater Lett 64(2223-2226), 2223-2226 (2010).
- [18] Dejene FB, Hossain FI, Mater Sci Semicond Process 71(73-81), 73-81 (2017).
- [19] Sharma P, Sharma RK, Mater Res Bull 95(69-77), 69-77 (2017).
- [20] Chauhan D, Yadav M, Tripathi S, Singh K, J Nanostruct Chem 12(61-71), 61-71 (2022).
- [21] Aziz SB, Hussein G, Abdulwahid RT, J Mater Sci Mater Electron 32(25172-25184), 25172-25184 (2021).
- [22] Ali G, Ikram M, Khan M, Ceram Int 46(6701-6710), 6701-6710 (2020).
- [23] Tang J, Zhang H, Yu X, J Alloys Compd 850(156653), 156653 (2021); https://doi.org/10.1016/j.jallcom.2020.156653
- [24] Yang Y, Zheng W, Cui H, Colloids Surf A 475(51-57), 51-57 (2015).
- [25] Mukherjee S, Ghosh M, Phys B Condens Matter 603(412722), 412722 (2021); https://doi.org/10.1016/j.physb.2020.412722
- [26] Wang X, Xu X, Choi SUS, J Thermophys Heat Transf 13(474-480), 474-480 (1999); https://doi.org/10.2514/2.6486
- [27] Pak BC, Cho YI, Exp Heat Transf 11(151-170), 151-170 (1998); https://doi.org/10.1080/08916159808946559
- [28] Choi SUS, ASME Int Mech Eng Congr Expo 66(99-105), 99-105 (1995).
- [29] Javed MS, Shahzadi S, Thermochim Acta 679(178352), 178352 (2019).
- [30] Bianco V, Manca O, Nardini S, Renew Sustain Energy Rev 14(2963-2972), 2963-2972

(2010).

- [31] Wang B, Zhou L, Peng X, Particuology 7(141-150), 141-150 (2009); https://doi.org/10.1016/j.partic.2009.01.007
- [32] Ding Y, Alias H, Wen D, Williams RA, Int J Heat Mass Transf 49(240-250), 240-250 (2006); https://doi.org/10.1016/j.ijheatmasstransfer.2005.07.009
- [33] Mishra P, Ghosh A, Mater Sci Eng B 256(114543), 114543 (2020).
- [34] Kumar S, Kumar M, Optik 127(1970-1975), 1970-1975 (2016).
- [35] Rahman MM, Asiri AM, RSC Adv 7(16810-16830), 16810-16830 (2017).
- [36] Zhang L, Zhou W, J Mater Sci Mater Electron 28(13775-13784), 13775-13784 (2017).
- [37] Venkatesan R, Ramachandran K, Spectrochim Acta A Mol Biomol Spectrosc 136(256-264), 256-264 (2015).
- [38] Saravanakumar K, Muthuraj V, J Alloys Compd 624(33-39), 33-39 (2015).
- [39] Kebede M, Pillai SC, Sol Energy Mater Sol Cells 200(110053), 110053 (2019).
- [40] Ozturk B, Gunes M, Renew Sustain Energy Rev 143(110859), 110859 (2021).
- [41] Qureshi ZA, Sulaiman SA, Renew Sustain Energy Rev 63(632-646), 632-646 (2016).
- [42] Ebrahimnia-Bajestan E, Safaei MR, Goodarzi M, Renew Sustain Energy Rev 76(1474-1492), 1474-1492 (2017).
- [43] Kang S, Choi H, J Sol Energy Eng 142(010801), 010801 (2020).
- [44] Sarkar J, Ghosh P, Adil A, Renew Sustain Energy Rev 43(164-177), 164-177 (2015); https://doi.org/10.1016/j.rser.2014.11.023
- [45] Akbari M, Hadianfard MJ, J Mol Liq 329(115441), 115441 (2021).
- [46] Sajid MU, Ali HM, Int J Heat Mass Transf 126(211-234), 211-234 (2018); https://doi.org/10.1016/j.ijheatmasstransfer.2018.05.021
- [47] Alawi OA, Sidik NAC, Appl Therm Eng 112(1119-1131), 1119-1131 (2017).
- [48] Mahbubul IM, Amalina MA, Nanoscale Res Lett 8(123), 123 (2013).
- [49] Godson L, Raja B, Lal DM, Wongwises S, Renew Sustain Energy Rev 14(629-641), 629-641 (2010); https://doi.org/10.1016/j.rser.2009.10.004
- [50] Mukherjee S, Ray D, Sol Energy 228(1-21), 1-21 (2021).
- [51] Arif AFM, Hilmi EA, Case Stud Therm Eng 14(100476), 100476 (2019).
- [52] Li Q, Xuan Y, Sci China Ser E 45(408-416), 408-416 (2002); https://doi.org/10.1360/02ye9047
- [53] Shahrul IM, Mamat R, Yusof TMT, Said MA, Appl Therm Eng 36(103-111), 103-111 (2012).
- [54] Kole M, Dey TK, J Phys D Appl Phys 43(315501), 315501 (2010); https://doi.org/10.1088/0022-3727/43/31/315501